

Suppression of Charge Density Wave by Substrate Induced Doping on $\text{TiSe}_2/\text{TiO}_2$ Heterostructure

Tao Jia,^{†,‡,§} Slavko N. Rebec,^{†,‡,§} Shujie Tang,[†] Kejun Xu,[‡] Hafiz M. Sohail,^{†,‡}
Makoto Hashimoto,[¶] Dong-Hui Lu,[¶] Robert G. Moore,[†] and Zhi-Xun Shen^{*,†,‡}

[†]*Stanford Institute for Materials and Energy Sciences, SLAC National Accelerator
Laboratory, Menlo Park, California 94025, USA*

[‡]*Geballe Laboratory for Advanced Materials, Departments of Physics and Applied Physics,
Stanford University, Stanford, California 94305, USA*

[¶]*Stanford Synchrotron Radiation Lightsource, SLAC National Accelerator Laboratory,
Menlo Park, California 94025, USA*

[§]*These two authors contributed equally to this work.*

E-mail: zxshen@stanford.edu

Abstract

Substrate engineering provides an opportunity to modulate the physical properties of quantum materials in thin film form. Here we report that TiSe_2 thin films grown on TiO_2 have unexpectedly large electron doping that suppresses the charge density wave (CDW) order. This is dramatically different from either bulk single crystal TiSe_2 or TiSe_2 thin films on graphene. The epitaxial TiSe_2 thin films can be prepared on TiO_2 via molecular beam epitaxy (MBE) in two ways: by conventional co-deposition using selenium and titanium sources, and by evaporating only selenium on reconstructed

TiO₂ surfaces. Both growth methods yield atomically flat thin films with similar physical properties. The electron doping and subsequent suppression of CDW order can be explained by selenium vacancies in the TiSe₂ film, which naturally occur when TiO₂ substrates are used. This is due to the stronger interfacial bonding that changes the ideal growth conditions. Our finding provides a way to tune the chemical potential of chalcogenide thin films via substrate selection and engineering.

Keywords

TiSe₂, charge transfer, substrate engineering, suppression of CDW

Introduction

Thin film growth using MBE has been shown to be a powerful tool for studies of correlated materials.¹⁻³ Physical properties of correlated thin films can be significantly changed through substrate selection and engineering. For instance, titanate substrates including SrTiO₃, anatase and rutile TiO₂ have been found to have multiple effects on FeSe films, including large and anisotropic strain, charge transfer, interfacial electron-phonon coupling and superconducting transition temperature enhancement.^{2,4-6} It is therefore interesting to test the effect of titanate substrates on other thin films of correlated electron systems.

Layered transition-metal dichalcogenides (TMDC) have been extensively studied due to their interesting physical properties, including the emergence of superconductivity and CDW order.^{7,8} Specifically, TiSe₂ has attracted significant interest due to the controversy over the driving force of its CDW order. TiSe₂ bulk single crystals undergo a phase transition at around 200 K into a CDW state characterized by the 3D commensurate ($2 \times 2 \times 2$) wave vector.⁹ There are multiple explanations of the origin of the CDW in TiSe₂, including band Jahn-Teller effect,¹⁰ exciton condensation^{11,12} and conventional Fermi-surface nesting.¹³ Monolayer thin films of TiSe₂ have been grown on bilayer graphene using MBE,

yielding similar band structure, and CDW with a 2D commensurate (2×2) wave vector. The CDW transition temperature for monolayer TiSe_2 on graphene is slightly higher than that of bulk crystals.^{14,15} In multilayer thin films of TiSe_2 on graphene, the CDW wave vector changes from 2D-like to 3D-like and the transition temperature decreases to bulk value as thickness increases.¹⁶ The intriguing physical properties of TiSe_2 make it an attractive testbed for the study of substrate effects on thin films.

In this work, we grew TiSe_2 on rutile TiO_2 (100) ($\text{TiSe}_2/\text{TiO}_2$) and bi-layer graphene ($\text{TiSe}_2/\text{graphene}$) substrates using MBE and characterized its electronic structure via angle-resolved photoemission spectroscopy (ARPES). We find that the TiSe_2 films on TiO_2 ($\text{TiSe}_2/\text{TiO}_2$) are heavily electron doped and do not show the signatures of a CDW in ARPES spectra. Furthermore, after depositing selenium on vacuum-annealed TiO_2 substrates (thereafter noted as $\text{Se}:\text{TiO}_2$), Se atoms reacts with the reconstructed substrate surface, and organizes into epitaxial films of TiSe_2 . Our experiments on $\text{TiSe}_2/\text{TiO}_2$ films provide a way to tune the chemical potential and change the ground state property of thin films through substrate engineering.

Electronic Band Structure

Previous researchers have reported the band structure of TiSe_2 (either in bulk form or $\text{TiSe}_2/\text{graphene}$),^{14,17} and the results of TiSe_2 bulk single crystals and $\text{TiSe}_2/\text{graphene}$ are very similar. Near the Fermi level (E_F), there is a pair of bands centered at the Γ point. At the M point, the bottom of an electron band reaches just below E_F . We measured the Fermi surface and band structure of $\text{TiSe}_2/\text{graphene}$ at ~ 20 K, shown in Fig 1(b, c). At this measurement temperature, $\text{TiSe}_2/\text{graphene}$ is in the CDW phase and the ARPES data clearly show that the hole bands at Γ are folded to M. There is little signal of the folding from the electron band at M to Γ , which is consistent with previous ARPES works.^{14,17} From the Fermi surface map we observe six tiny pockets formed by electron bands at M. These

results are consistent with the previous research on TiSe₂/graphene.^{14–16}

The Fermi surface and band structure of TiSe₂/TiO₂ at the same measurement temperature of 20 K, shown in Fig 1(e-f), exhibit a few stark differences from those of TiSe₂/graphene. The bands are no longer folded, indicating the lack of CDW order. Also the electron pockets are much larger for TiSe₂/TiO₂, representing a doping of $n \approx 0.16(2)$ electron per unit cell, calculated from the Fermi surface volume. In contrast, TiSe₂/graphene has a doping of merely $n = 0.02$ over the perfectly stoichiometric compound (see Fig 1(b)). The doping of TiSe₂/graphene is nonzero possibly due to Se vacancies. Besides those two features, below the main electron band near the M point (denoted as α in Fig. 1(f)) there is a weaker copy of the band around 100 meV below the main band and crossing the Fermi level, denoted as α' band. This “copy” band is more clearly seen in the second energy derivative of the ARPES spectra in Supplemental Figure 2. This cannot be attributed to the quantum well effects in the finite-thickness films, as the energy difference between α and α' is thickness independent up to 24 monolayers (ML) (see Supplemental Fig. 1). Further work needs to be done to explain the origin of the band α' .

All the three features mentioned above, including lack of CDW, large electron doping and the “copy” band α' at M, have little thickness dependence from 3ML to 24ML, as is demonstrated in Supplemental Fig. 1.

Rutile TiO₂ (100) surface undergoes a (3×1) reconstruction above 670 °C. During this process parts of surface atoms are lost, leading to a terraced surface with exposed atoms of titanium.¹⁸ Surprisingly, after annealing the rutile TiO₂ substrate above the surface reconstruction temperature in vacuum, we can grow epitaxial thin films of TiSe₂ by only depositing Se. Given that, we speculate that Se atoms react with the Ti atoms exposed to vacuum due to the reconstruction, and form TiSe₂ (denoted before as Se:TiO₂). The electronic band structure of Se:TiO₂, shown in Fig 1(i), is very similar to that of TiSe₂/TiO₂ grown by co-deposition of Se and Ti. As in TiSe₂/TiO₂, there is no band folding between Γ and M, which indicates the suppression of CDW, and very large electron doping level of

$n \approx 0.22$ electron/unit cell. Also below the main band α near M there is a “copy” band α' , shown in Fig. 1(i), similar to the case of $\text{TiSe}_2/\text{TiO}_2$.

We further compared the band structure of $\text{TiSe}_2/\text{graphene}$ and the TiSe_2 films grown on TiO_2 . Figure 2 (a-c) display the deeper valence bands for 1ML $\text{TiSe}_2/\text{graphene}$, 6ML $\text{TiSe}_2/\text{TiO}_2$ and $\text{Se}:\text{TiO}_2$, respectively. In $\text{TiSe}_2/\text{TiO}_2$, there are two bands which share similar dispersion but are separated by 350 meV. There is a hint of the band γ' in $\text{Se}:\text{TiO}_2$ as well, but the signal is much weaker. The origin of the band γ' in TiSe_2 films on TiO_2 substrate needs further work to elucidate. Besides this difference, the vast majority of band features are similar with the exception of a chemical potential shift in the cases of $\text{TiSe}_2/\text{TiO}_2$ and $\text{Se}:\text{TiO}_2$.

Figure 2 (d) shows the core level spectra of $\text{TiSe}_2/\text{graphene}$, 7ML $\text{TiSe}_2/\text{TiO}_2$ and $\text{Se}:\text{TiO}_2$. The Se double peaks are similar for all three systems in both position and magnitude. The Ti peaks for $\text{TiSe}_2/\text{TiO}_2$ and $\text{Se}:\text{TiO}_2$ are shifted towards lower binding energy and have slightly different shapes. Previous reports discuss the creation of Ti^{3+} states on the surface of vacuum annealed TiO_2 ,¹⁹ which will cause additional shoulders with lower binding energy in the Ti $2p$ X-ray photoemission spectra. Thus we may explain the energy shift in the core level spectra of $\text{TiSe}_2/\text{TiO}_2$ and $\text{Se}:\text{TiO}_2$ by the formation of Ti^{3+} states. However, this energy shift is also seen for 7ML $\text{TiSe}_2/\text{TiO}_2$, where the signal from the Ti^{3+} ions in TiO_2 substrate should diminish. With an estimated probing depth of 0.6 nm,²⁰ the Ti^{3+} signature from TiO_2 should diminish by a factor of 1,000 for a 7ML film compared to the bare TiO_2 substrate. This is in contradiction to the observation that $\text{Se}:\text{TiO}_2$ and $\text{TiSe}_2/\text{TiO}_2$ have similar Ti $2p$ photoemission spectra. Such an observation suggests that the electron doping on $\text{TiSe}_2/\text{TiO}_2$ may induce Ti^{3+} ions in TiSe_2 films as well. The measurement of deeper valence band and core level further verifies that the films on TiO_2 , grown by either Se deposition or Ti/Se co-deposition, are TiSe_2 .

Surface Characterization

Next we continue to characterize the quality of the TiSe_2 films on TiO_2 . TiSe_2 is a layered material with hexagonal lattice and a lattice constant of $a = 0.354$ nm. TiO_2 (100) surface is rectangular with lattice parameters $a = 0.459$ nm, $c = 0.295$ nm. We can view the (100) surface of the substrate as a distorted hexagonal lattice, but this still leads to a large and anisotropic strain of more than 20%, as is shown in Figure 3(a). Therefore, it seems unlikely to achieve layer-by-layer growth of $\text{TiSe}_2/\text{TiO}_2$. Nonetheless, Reflective High Energy Electron Diffraction (RHEED) and Scanning Tunneling Microscope (STM) topography show epitaxial growth of TiSe_2 for both $\text{TiSe}_2/\text{TiO}_2$ and $\text{Se}:\text{TiO}_2$. The strain is $< 2\%$ determined by RHEED diffraction pattern. The RHEED images, oscillations of RHEED intensity and STM topography are shown in Figure 3(d-i). Intriguingly, we can see RHEED intensity “oscillations” for $\text{Se}:\text{TiO}_2$, even though the reaction is between deposited Se atoms and Ti atoms on the substrate. These results, combined with the clarity in the ARPES spectra, demonstrate the excellent surface quality of the film for both Se deposition and co-deposition.

Analysis

With the chemical composition and surface quality verified for $\text{TiSe}_2/\text{TiO}_2$ and $\text{Se}:\text{TiO}_2$, we now turn back to the explanation of their electronic band structures. The two main features of TiSe_2 films on TiO_2 are the large electron doping and the suppression of the CDW.

Currently the origin of the CDW in TiSe_2 is still under debate. Some attribute it to a Peierls charge density wave, which is created by a spontaneous crystal distortion driven by the electron-phonon interaction.^{9,13} Many others describe the low-temperature phase as excitonic condensation where electrons and holes combine into excitons which then Bose condense.^{11,12} In either case, it is expected that external electron doping will suppress the CDW. For the case of a Peierls CDW, increasing carrier density will alter the Fermi surface nesting conditions and promote superconductivity, which competes with the CDW. For an

excitonic condensate, doping will break the balance between electrons and holes and hence restraining the condensation. Previous researchers have doped TiSe_2 by Cu intercalation^{21,22} and ionic liquid gating,²³ and both methods lead to the destruction of the CDW and the formation of a superconductivity dome in the phase diagram.

The most unusual aspect of this system is the magnitude of its doping. Changing post-growth annealing temperature of TiSe_2 can control Se vacancy defects, which may act as electron dopants.²⁴ By default we do post-growth annealing at the growth temperature, which is 200 °C for $\text{TiSe}_2/\text{graphene}$, and 360-380 °C for $\text{TiSe}_2/\text{TiO}_2$. Therefore, we systematically compare the films of all 3 growth modes with different post-growth annealing temperatures to investigate its effect on the electronic properties. Figure 4(e-f) shows the Fermi surface of $\text{TiSe}_2/\text{graphene}$ after low and high temperature post-growth annealing. The Fermi surface becomes significantly larger after a mere 50°C increase in annealing temperature (from 200 °C to 250 °C), indicating that the high temperature post-growth annealing can create Se vacancies and induce electron doping. Nevertheless, if we immediately quench $\text{TiSe}_2/\text{TiO}_2$ and $\text{Se}:\text{TiO}_2$ films to temperatures below 200 °C after growth, the Fermi surface volume is still much larger than the case of $\text{TiSe}_2/\text{graphene}$, which is clear if we compare Fig. 4(a, c, e). When the doping level is higher than 0.15 electron/Ti atom, as shown in Fig 4 (a-d,f), the CDW order is destroyed. This shows that TiO_2 substrate, directly or indirectly, induces large doping level into TiSe_2 .

It is plausible to assume the interfacial charge transfer from work function difference as the origin of the electron doping in TiSe_2 films on TiO_2 . The work function difference between TiSe_2 ²⁵ and TiO_2 ²⁶ is as large as ~ 1.2 eV, which may enable direct interfacial transfer of electrons from TiO_2 substrate to TiSe_2 film. However, the effects of interfacial charge transfer are strongly limited by the thickness of films due to electronic screening from the films. Since there is no thickness dependence of the Fermi surface size up to 24ML (see Supplemental Fig. 1), the work function induced interfacial charge transfer cannot be the main reason for the electron doping for TiSe_2 films on TiO_2 .

Below we consider an indirect effect from the TiO_2 substrate: the strong interfacial bonding between TiSe_2 and TiO_2 leads to a growth window with higher growth temperature. More Se vacancies are created during growth under this condition compared to the case of $\text{TiSe}_2/\text{graphene}$, resulting in electron doping and suppression of CDW in TiSe_2 .

The ideal growth temperature for $\text{TiSe}_2/\text{TiO}_2$ and $\text{Se}:\text{TiO}_2$ is consistently higher than that for $\text{TiSe}_2/\text{graphene}$. The ideal growth temperature for $\text{TiSe}_2/\text{TiO}_2$ and $\text{Se}:\text{TiO}_2$ is between 350-380 °C, below which the growth yields amorphous films. On the other hand, if we grow $\text{TiSe}_2/\text{graphene}$ at any temperature above 250 °C, there will be no formation of new RHEED streaks. This means that at this temperature, the Se re-evaporation rate is too high to allow the growth of TiSe_2 on graphene. This substrate-induced growth temperature difference between graphene and TiO_2 can be explained by the growth dynamics. Graphene provides much weaker interfacial interaction, therefore the ideal growth temperature is low. In contrast, TiO_2 surface tends to form stronger bonds with TiSe_2 on the interface, thus a higher growth temperature is needed to provide sufficient diffusion rate necessary to form pristine films.

At the growth temperature of $\text{TiSe}_2/\text{TiO}_2$ and $\text{Se}:\text{TiO}_2$ (380 °C), Se re-evaporation can be very strong, according to the results of $\text{TiSe}_2/\text{graphene}$ from both Fig 4(f) and a previous STM study.²⁴ As a result, during the growth process, there is already strong Se re-evaporation, leading to Se deficiency and electron doping, even though we are growing in a Se-rich regime. However, the heavily doped $\text{TiSe}_2/\text{TiO}_2$ and $\text{Se}:\text{TiO}_2$ films generally show superior ARPES spectrum than the $\text{TiSe}_2/\text{graphene}$ films with higher post-growth annealing temperatures. The sharper ARPES is indicative of improved crystalline quality. Thus the enhanced substrate-film bonding yields significant selenium defects and therefore large electron doping, while maintaining superior crystallinity overall.

To summarize, we can explain the suppression of charge density wave order by the large electron doping, and explain the electron doping by Se vacancies created by substrate induced change of growth conditions. The doping is because of the change of growth condition

instead of a direct effect of substrate, which can explain why this effect is independent of film thickness up to 24ML.

Conclusion

We grew TiSe_2 on rutile TiO_2 (100) substrates using MBE, in which substrate effects provide large doping to TiSe_2 that suppresses CDW order. This demonstrates that, in the course of tuning the chemical potential of thin film samples, we can add a large and flexible offset by selecting and engineering the substrate. The substrate-induced doping, compared to conventional methods including alkali metal atom intercalation and ionic liquid gating, provides a cleaner way of doping thin films in that it does not provide external impurities to the system. In addition, our results demonstrate that pristine TiSe_2 thin films can form on reconstructed TiO_2 substrate after Se deposition, which may pave the way to new growth methods of other chalcogenide/oxide heterostructure, and improve our understanding of the chemical property of the reconstructed surface of oxides.

Previous studies doped electrons into TiSe_2 to a maximal level of ~ 0.06 electron per unit cell, and observed superconductivity.^{21,22,27} In contrast, TiSe_2 films on TiO_2 reported in this work has a doping of >0.16 electron per unit cell without any external intercalation or liquid gating, entering into an unexplored regime in the TiSe_2 phase diagram. It would be interesting to do further experiments to investigate into the transport properties of TiSe_2 films on TiO_2 . We also plan to apply similar substrate engineering methods to other heterostructures of correlated materials as a powerful way to explore further in the phase diagrams.

Methods

Growth

For $\text{TiSe}_2/\text{TiO}_2$, Shinkosha STEP TiO_2 (100) substrates were mounted on a molybdenum sample holder with silver paste and placed into an MBE chamber. The base pressure of the MBE chamber was 8×10^{-11} torr. Substrates were then degassed at 450 - 650 °C, and cooled down to 360 °C for growth. Ultra-high purity titanium (99.995%) and selenium (99.999%) were then deposited onto the substrate. The crystallinity was examined using reflection high energy electron diffraction (RHEED). The films were then annealed at 380°C for 2 hours (except for the ones noted with “Low Temperature Anneal” in Fig. 4). The growth conditions of $\text{Se}:\text{TiO}_2$ is similar to that of $\text{TiSe}_2/\text{TiO}_2$, except that before growth the substrates are annealed at 810 - 860 °C for 30 minutes in addition to degassing, and that only Se cell is used during the growth.

For $\text{TiSe}_2/\text{graphene}$, the TiSe_2 films were grown by MBE on bilayer graphene (BLG) epitaxially grown on 6H-SiC.²⁸ The growth temperature is at around 200 °C. The films were then annealed at growth temperature °C for 2 hours (except for the ones noted with “High Temperature Anneal” in Fig. 4).

The successful growth of $\text{Se}:\text{TiO}_2$ relies on the preparation of substrate. TiO_2 rutile (100) surface undergoes a (3×1) reconstruction at temperatures above 670 °C, exposing Ti atoms from surface layers to vacuum.¹⁸ Only when we pre-anneal the substrate to the temperature range within 810 - 860 °C will we grow epitaxial films with clear ARPES spectra. If pre-annealing temperature is too low, the films will not form, possibly because there are not enough Ti atoms exposed to vacuum. If pre-annealing temperature is above 860 °C, the films will show ARPES spectra with very broad bands and scattered intensity, resulting from a very rough substrate surface.

On a side note, we want to alert chalcogenide thin film growers that substrate-film reaction and the resulting $\text{Se}:\text{TiO}_2$ may accidentally occur during the process of preparing other

chalcogenide/titanate heterostructures, as the condition for the formation of Se:TiO₂ is in close proximity with the growth condition of many other chalcogenide films. For example, Se:TiO₂ can act as an impurity phase for the growth of FeSe/TiO₂ if the substrate is pre-annealed at temperatures above 790 °C, giving hexagonal lattice with Fermi surfaces and electronic structures very similar to what is reported in this work. Similar mechanisms of TiSe₂ formation may also happen for chalcogenide films on other titanate substrates including SrTiO₃ and anatase TiO₂.

Measurement

After growth, the films were transferred *in situ* to the ARPES end station of the Stanford Synchrotron Radiation Lightsource beamline 5-2. The base pressure in the ARPES chamber was better than 4×10^{-11} torr. Circular right polarization was used during the measurement. The high symmetry cuts were done with photon energy of 46 eV, and the energy resolution is better than 25 meV; Reciprocal space maps were measured using photon energy of 82 eV, and the energy resolution is better than 44 meV. The angular resolution is better than 0.4°.

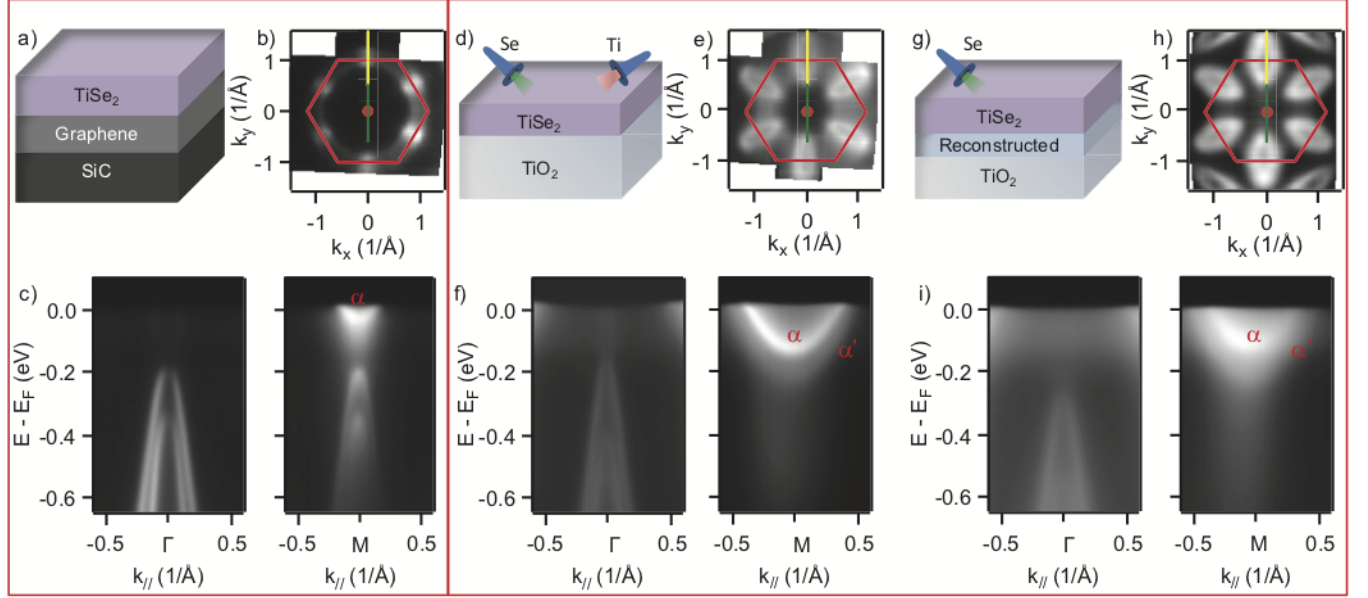


Figure 1: (a) sketch of the heterostructures for $\text{TiSe}_2/\text{graphene}$. (b) photoemission intensity maps near $E = E_F$ for an energy window of 10 meV for 1ML $\text{TiSe}_2/\text{graphene}$. The yellow and green lines represent the direction of high-symmetry scans through zone center and zone boundary, respectively. (c) band structure for 1ML $\text{TiSe}_2/\text{graphene}$ along the high symmetry scans across the zone center (green line in (b, e, h)) and the zone boundary (yellow line in (b, e, h)). (d, e, f) same as (a, b, c), except that the sample for (e) is 15ML $\text{TiSe}_2/\text{TiO}_2$ and the sample for (f) is 10.5ML $\text{TiSe}_2/\text{TiO}_2$. (g, h, i) the same as (a, b, c), except that the samples are Se: TiO_2 . All data were taken at 20 K. (b, e, h) taken with 82 eV photons, (c, f, i) taken with 46 eV photons.

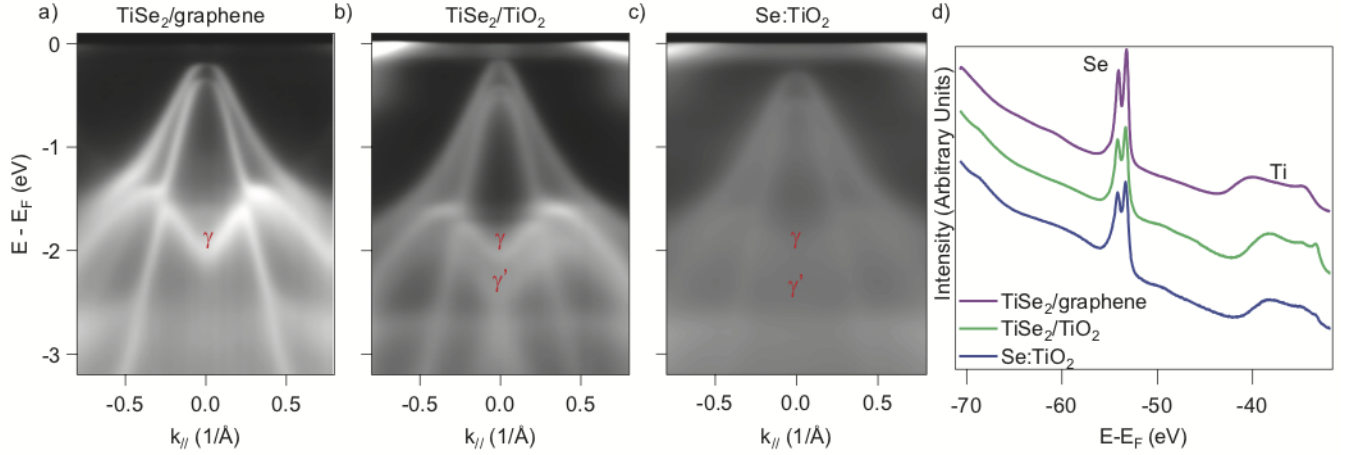


Figure 2: (a) The band structure for 1ML $\text{TiSe}_2/\text{graphene}$ at the zone center (see the green line in Fig 1(b)); (b) The band structure for 10.5ML $\text{TiSe}_2/\text{TiO}_2$ at the zone center; (c) The band structure for $\text{Se}:\text{TiO}_2$ at zone center; (d) The core level photoemission intensity of 1ML $\text{TiSe}_2/\text{graphene}$, 7ML $\text{TiSe}_2/\text{TiO}_2$ and $\text{Se}:\text{TiO}_2$. All data were taken at 20 K. (a-c) taken with 46 eV photons, (d) taken with 82 eV photons.

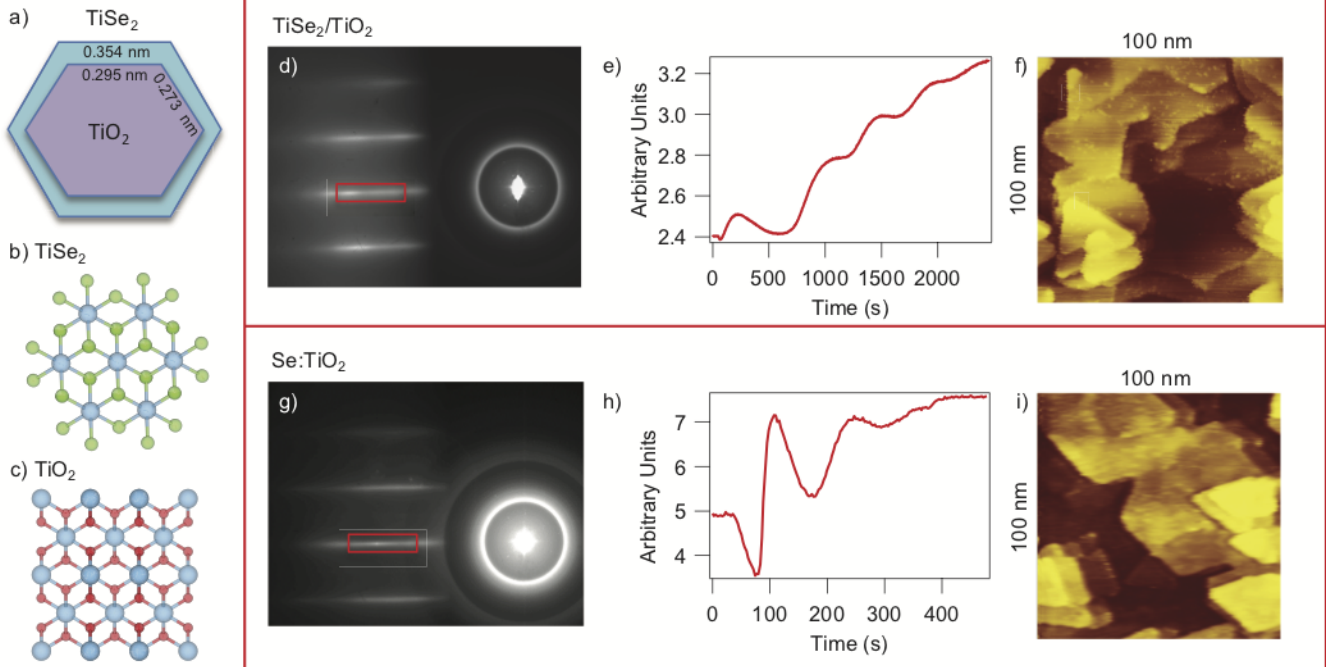


Figure 3: (a) Comparison between the lattices of TiSe_2 and TiO_2 ; (b) The (0001) projection of the atomic structure of TiSe_2 , where blue spheres indicate Ti atoms, and green spheres indicate Se atoms; (c) The (100) projection of the atomic structure of TiO_2 , where blue spheres indicate Ti atoms, and red balls indicate Oxygen atoms; (d-f) Surface characterization of $\text{TiSe}_2/\text{TiO}_2$ films: (d) RHEED pattern for a 21ML sample; (e) The evolution of RHEED intensity integrated from the red rectangle versus time during growth for a 15ML sample; (f) the STM topography measurement for the same sample as (e); (g-i) The same as (d-f), but for $\text{Se}:\text{TiO}_2$ film.

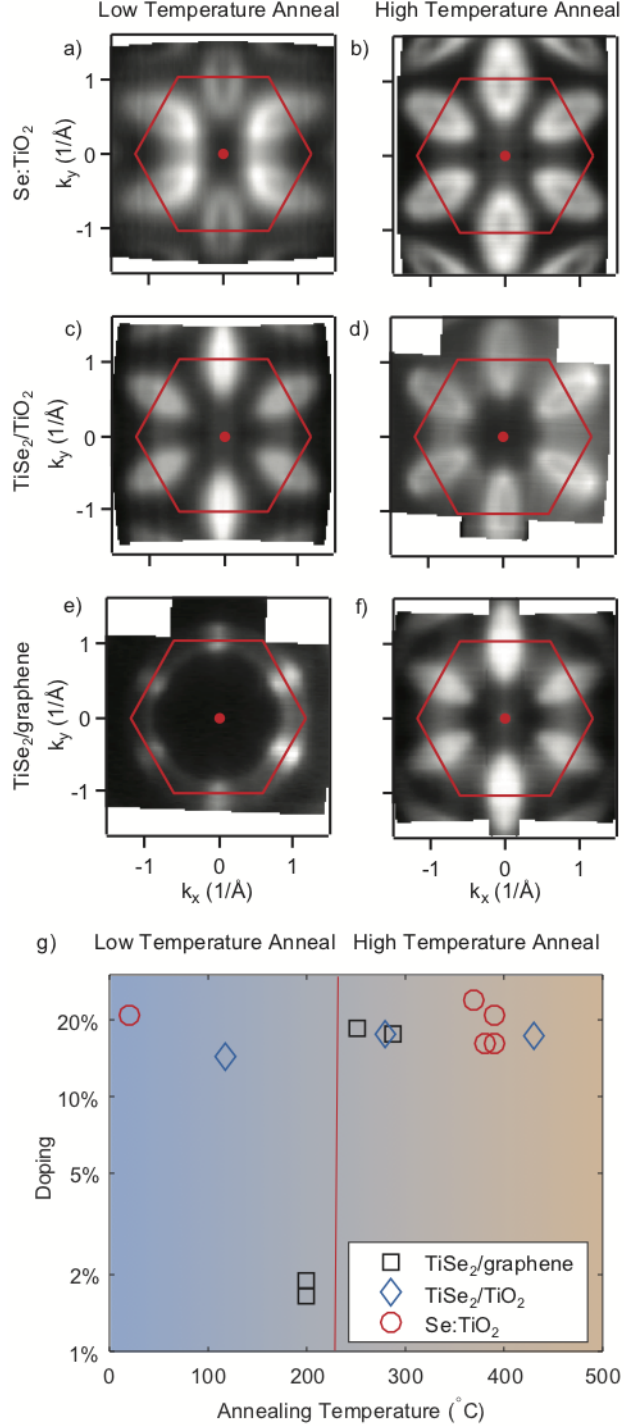


Figure 4: (a-f) ARPES intensity mapping near $E = E_F$ for an energy window of 10 meV, measured at 20 K. The Brillouin zone of bulk TiSe_2 is plotted in red for comparison. (a) Se:TiO_2 , quenched to 30 °C immediately after growth; (b) Se:TiO_2 , annealed at 390 °C; (c) $\text{TiSe}_2/\text{TiO}_2$, 9ML, quenched to 120 °C; (d) $\text{TiSe}_2/\text{TiO}_2$, 15ML, annealed at 280 °C; (e) $\text{TiSe}_2/\text{graphene}$, 1ML, annealed at 220 °C; (f) $\text{TiSe}_2/\text{graphene}$, 1ML, annealed at 280 °C. (g) The relationship between doping level and annealing temperature for Se:TiO_2 , $\text{TiSe}_2/\text{TiO}_2$ and $\text{TiSe}_2/\text{graphene}$. The red line is a guide of the eye indicating the separation between Low Temperature Anneal and High Temperature Anneal. All data taken with 82 eV photons.

Acknowledgement

We would like to thank B. Moritz, C.-J. Jia, Y. He, and S.-D. Chen for valuable discussions. This work is supported by the Department of Energy, Office of Science, Basic Energy Sciences, Materials Sciences and Engineering Division, under Contract DE-AC02-76SF00515. Use of the Stanford Synchrotron Radiation Lightsource, SLAC National Accelerator Laboratory, is supported by the U.S. Department of Energy, Office of Science, Office of Basic Energy Sciences, also under Contract No. DE-AC02-76SF00515.

References

- (1) Ohtomo, A.; Hwang, H. Y. *Nature* **2004**, *427*, 423–426.
- (2) Wang, Q.-Y. et al. *Chinese Physics Letters* **2012**, *29*, 037402.
- (3) Logvenov, G.; Gozar, A.; Bozovic, I. *Science* **2009**, *326*, 699–702.
- (4) Lee, J. J.; Schmitt, F. T.; Moore, R. G.; Johnston, S.; Cui, Y.-T.; Li, W.; Yi, M.; Liu, Z. K.; Hashimoto, M.; Zhang, Y.; Lu, D. H.; Devereaux, T. P.; Lee, D.-H.; Shen, Z.-X. *Nature* **2014**, *515*, 245–248.
- (5) Ding, H.; Lv, Y.-F.; Zhao, K.; Wang, W.-L.; Wang, L.; Song, C.-L.; Chen, X.; Ma, X.-C.; Xue, Q.-K. *Phys. Rev. Lett.* **2016**, *117*, 067001.
- (6) Rebec, S. N.; Jia, T.; Zhang, C.; Hashimoto, M.; Lu, D.-H.; Moore, R. G.; Shen, Z.-X. *Phys. Rev. Lett.* **2017**, *118*, 067002.
- (7) Rossnagel, K. *Journal of Physics: Condensed Matter* **2011**, *23*, 213001.
- (8) Manzeli, S.; Ovchinnikov, D.; Pasquier, D.; Yazyev, O. V.; Kis, A. *Nature Reviews Materials* **2017**, *2*, 17033.
- (9) Di Salvo, F. J.; Moncton, D. E.; Waszczak, J. V. *Phys. Rev. B* **1976**, *14*, 4321–4328.

- (10) Hughes, H. P. *Journal of Physics C: Solid State Physics* **1977**, *10*, L319.
- (11) Wilson, J. A. *Solid State Communications* **1977**, *22*, 551 – 553.
- (12) Cercellier, H.; Monney, C.; Clerc, F.; Battaglia, C.; Despont, L.; Garnier, M. G.; Beck, H.; Aebi, P.; Patthey, L.; Berger, H.; Forró, L. *Phys. Rev. Lett.* **2007**, *99*, 146403.
- (13) Suzuki, N.; Yamamoto, A.; Motizuki, K. *Solid State Communications* **1984**, *49*, 1039 – 1043.
- (14) Chen, P.; Zhang, Y.; Chou, M. Y.; Hussain, Z. *Nature Communications* **2015**, 8–12.
- (15) Sugawara, K.; Nakata, Y.; Shimizu, R.; Han, P.; Hitosugi, T.; Sato, T.; Takahashi, T. *ACS Nano* **2016**, *10*, 1341–1345.
- (16) Chen, P.; Chan, Y.-H.; Wong, M.-H.; Fang, X.-Y.; Chou, M. Y.; Mo, S.-K.; Hussain, Z.; Fedorov, A.-V.; Chiang, T.-C. *Nano Letters* **2016**, *16*, 6331–6336.
- (17) Rossnagel, K.; Kipp, L.; Skibowski, M. *Phys. Rev. B* **2002**, *65*, 235101.
- (18) Diebold, U. *Surface Science Reports* **2003**, *48*, 53 – 229.
- (19) Guillemot, F.; Port, M.; Labrugre, C.; Baquey, C. *Journal of Colloid and Interface Science* **2002**, *255*, 75 – 78.
- (20) Lindau, I.; Spicer, W. *Journal of Electron Spectroscopy and Related Phenomena* **1974**, *3*, 409 – 413.
- (21) Morosan, E.; Zandbergen, H. W.; Dennis, B. S.; Bos, J. W. G.; Onose, Y.; Klimczuk, T.; Ramirez, A. P.; Ong, N. P.; Cava, R. J. *Nature Physics* **2006**, *2*, 544.
- (22) Zhao, J. F.; Ou, H. W.; Wu, G.; Xie, B. P.; Zhang, Y.; Shen, D. W.; Wei, J.; Yang, L. X.; Dong, J. K.; Arita, M.; Namatame, H.; Taniguchi, M.; Chen, X. H.; Feng, D. L. *Phys. Rev. Lett.* **2007**, *99*, 146401.

- (23) Li, L. J.; O'Farrell, E. C. T.; Loh, K. P.; Eda, G.; Özyilmaz, B.; Castro Neto, A. H. *Nature* **2015**, *529*, 185.
- (24) Peng, J.-P.; Guan, J.-Q.; Zhang, H.-M.; Song, C.-L.; Wang, L.; He, K.; Xue, Q.-K.; Ma, X.-C. *Phys. Rev. B* **2015**, *91*, 121113.
- (25) Liu, Y.; Stradins, P.; Wei, S.-H. *Science Advances* **2016**, *2*.
- (26) Imanishi, A.; Tsuji, E.; Nakato, Y. *The Journal of Physical Chemistry C* **2007**, *111*, 2128–2132.
- (27) Qian, D.; Hsieh, D.; Wray, L.; Morosan, E.; Wang, N. L.; Xia, Y.; Cava, R. J.; Hasan, M. Z. *Phys. Rev. Letters* **2007**, *117007*, 2–5.
- (28) Wang, Q.; Zhang, W.; Wang, L.; He, K.; Ma, X.; Xue, Q. *Journal of Physics: Condensed Matter* **2013**, *25*, 095002.